Aerodynamic Performance and Flow Structure Studies of a Low Reynolds Number Airfoil

Fei-Bin Hsiao,* Chin-Fung Liu,† and Zen Tang‡
National Cheng Kung University, Tainan, Taiwan

The aerodynamic performance and flow structures of a model with a NACA 63_3-018 airfoil section are studied experimentally in a wind tunnel. The pressure distributions, boundary-layer profiles, and corresponding aerodynamic properties are measured at various angles of attack, and at the Reynolds number range from 300,000 to 774,000 based on the wing chord. Hot-wire anemometry and smoke wire technique are also applied for performing the flow measurements and visualization, respectively. Data indicate that the flowfield over the airfoil appears to be transitional in the operating range. The flow starts to be separated from the airfoil surface after the pressure gradient becomes positive and then is reattached to form a laminar separation bubble. The spectral analysis of the fluctuating velocities in the recirculating bubble region also clearly ascertains the existence of prevailing eddies. Meanwhile, the hysteresis phenomenon in the nonlinear range of the lift curves with angle of attack is significantly noted, especially in the low Reynolds number range.

Nomenclature

AOA	= angle of attack
atm	= atmospheric pressure
C	= chord
C_d	= section drag coefficient
C_l	= section lift coefficient
C_p	= pressure coefficient
P_t	= total pressure
Re_c	= Reynolds number based on chord
U_{bl}	= boundary-layer velocity
U_{edge}	= boundary-layer edge velocity
X	= coordinate along the chord line
Y	= coordinate normal to the chord line
δ	= boundary-layer thickness
δ_b	= boundary-layer separation thickness

Introduction

THERE are a large number of aircraft, such as remotely piloted vehicles, sailplanes, ultralight airplanes, etc., which usually fly at a Reynolds number ranging from 10,000 to 1,000,000, based on the mean aerodynamic chord.[1] According to boundary-layer theory, the flowfield in this Reynolds number range appears to be within the transition from laminar to turbulent flow. Because of increasing interest and importance, the investigations of the aerodynamic properties on a wing have drawn much attention in recent years.[2,3] Numerous researchers have pointed out that not only the flow structures over the wing are complex[4] but also the flow phenomena behave diversely for different geometric wings.[3,5] The flowfield in the low Reynolds number range may include the occurrence of the laminar and turbulent separation, the separation bubble structure, and the turbulent reattachment.[6] When a wing with a low angle of attack passes through a laminar freestream at a transitional Reynolds number, the flow on the upper wing surface will keep laminar from the leading edge to the point before the pressure gradient becomes positive. Beyond that point, the flow may or may not go through natural transition, depending upon the parameters such as the Reynolds number, the freestream turbulence, and some possible effects.[1] If transition does not occur, then with further downstream the laminar boundary layer will subsequently encounter a strong adverse pressure gradient such that the flow starts to be separated from the wing surface. The process of transition to turbulence then occurs due to shear layer instabilities and a violent flow mixing.[4] If the momentum exchange near the wall is strong enough, the turbulent boundary layer may be reattached to the wing surface to form a separation bubble. Before the reattached turbulent boundary layer reaches the trailing edge, a turbulent separation would take place if the flow cannot sustain the strong adverse pressure gradient in the rear portion of the airfoil. A literature survey indicates that the lift curve hysteresis is an important phenomenon.[3,5,7] It is clear that the behavior of the hysteresis phenomenon is related to the existence of the separation bubble, which is governed by the flow separation and transition over the wing. Hysteresis is of practical importance because it will result in producing different aerodynamic performance such as C_l, C_d, and C_l/C_d. Meanwhile, it then will substantially affect the static, dynamic, or aeroelastic stability of the entire vehicle. It could also affect the recovery from stall and/or spin flight conditions. Therefore, the successful management of the boundary-layer development in a low Reynolds number vehicle design is very crucial. It is suggested to carry out more wind-tunnel tests before this problem can be appropriately handled, either by theoretical analysis or numerical computation.[8-10]

The main goal of this paper is to present the aerodynamic properties and the flow structure characteristics of a model with a NACA 63_3-0.18 airfoil in the transitional Reynolds number range between 300,000 and 774,000. The measurements will cover the static pressure distributions along the chordwise direction and the streamwise boundary-layer mean

Received April 23, 1987; presented as Paper 87-1267 at the AIAA 19th Fluid Dynamics, Plasma Dynamics, and Lasers Conference, Honolulu, HI, June 8-10, 1987; revision received Dec. 16, 1987.

*Assistant Professor. Member AIAA.
†Ph.D. Candidate, Institute of Aeronautics and Astronautics.
‡Research Assistant, Institute of Aeronautics and Astronautics.

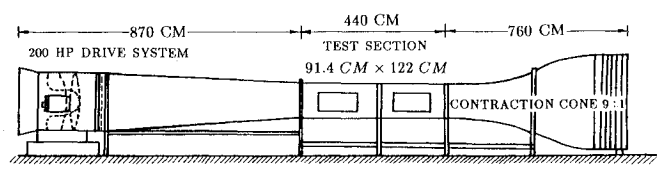

Fig. 1 Subsonic wind tunnel.

velocity profiles associated with the energy spectra of the fluctuating velocities. The corresponding aerodynamic parameters such as lift and drag coefficients will be determined as well. Besides, the flow visualization by using smoke wire technique is also performed in a smoke tunnel to investigate the flow structures during the separation.

Apparatus and Procedure

The experiment is conducted in an open, in-draft subsonic wind tunnel, with a 3 × 4 ft test section as shown in Fig. 1. The nozzle contraction ratio is 9:1, and five fine-mesh screens are installed in the settling chamber for managing the freestream turbulence. The velocity in the test section varies between 5 and 35 m/s. The turbulence intensity is about 0.25% within the operating range. The model is vertically mounted in the test section and is restricted on both ends with flat plates. It is made of aluminum alloy, and its cross section is a NACA 63_3-018 airfoil. The chord of the model is 1 ft, and the span is 2 ft. It is manufactured to accommodate five pressure taps in the spanwise direction and 29 taps staggered along the chordwise direction at the semispan on both faces of the model. The inside diameter of each tap is less than 1 mm. Flow visualization is carried out in a smoke tunnel with a 20 × 40 cm test section, as shown in Fig. 2. Smoke wire technique is used to visualize the flow separation development over the model by photography and video tape recording. Seven fine-mesh screens are installed in the settling chamber. The block diagram of the experimental setup is shown in Fig. 3. A PDP $11/23^+$ computer is used as the control unit along with a data acquisition system ANALOGIC ANDS 5400. Pressure distributions are obtained through the scanivalve to transmit the pressure data for digitizing and processing to get lift coefficients. A wake rake, made of 130 colinear total pressure tubes 1.5 mm in diameter and three out-of-plane static ports, is placed 1.5 ft downstream of the airfoil trailing edge to measure the drag force by using momentum defect method.[11] The total pressure tubes are arranged at intervals of 4 mm. To measure the boundary-layer mean velocity profiles along downstream, a flattened total pressure tube with 0.2 mm opening is used. Information regarding the velocity fluctuations is taken via a TSI 1050 constant-temperature hot-wire anemometer. A single hot wire is used as a sensor for investigating the eddy structures in the recirculating bubble region. It is mounted on a computer-controlled traversing mechanism that can be driven in accuracy up to 0.01 mm per step. The velocity fluctuating signals are directly fed into a B&K 2032 signal analyzer to obtain the energy spectra.

Results and Discussion

Flow Visualization

Figure 4 shows a sequence of flow visualization photographs with angle of attack at the Reynolds number of 15,400. The flow patterns for angles of attack less than 3 deg illustrate that the flow over the wing seems to keep laminar even after the maximum thickness point, whereas at higher angle of attack, due to shear layer instabilities, large-scale vortices are observed on the upper surface, which are shedded rearward into wake region. The wake region behind the wing is getting wider when the angle of attack is increased. At very high angle of attack, say 24 deg, the leading-edge separation is clearly revealed. Since the separation zone extends downward into the wake region without reattachment, it is a relevant case that the Reynolds number is in the subcritical range.[7] When the Reynolds number is increased to 55,000, a separation bubble is significantly observed, as shown in Fig. 5 for some flow patterns. A closed darkened area right adjacent to the upper surface depicts the location of the bubble. It indicates that the tested Reynolds number is now beyond the subcritical range. Figure 5a shows the bubble occurrence at zero angle of attack. It starts about at 50% chord and occupies approximately 30% chord length. At higher angle of attack (Figs. 5b and 5c), the bubble moves upstream and shrinks its length. But for the 9 deg angle of attack case (Fig. 5d), the bubble can hardly be discerned.

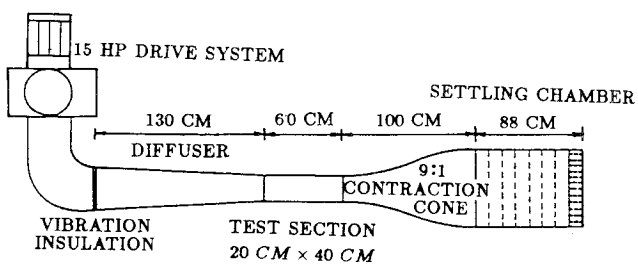

Fig. 2 Smoke tunnel.

Pressure Distributions and Aerodynamic Characteristics

Figure 6 depicts the chordwise distributions of the pressure coefficient for the upper and the lower surface at the Reynolds

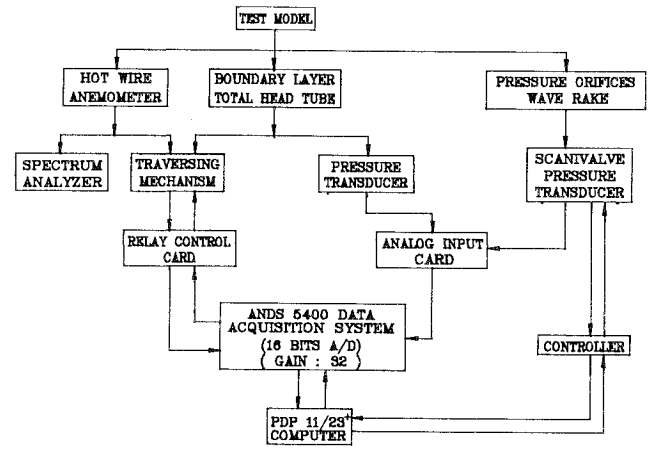

Fig. 3 Block diagram of the experiment.

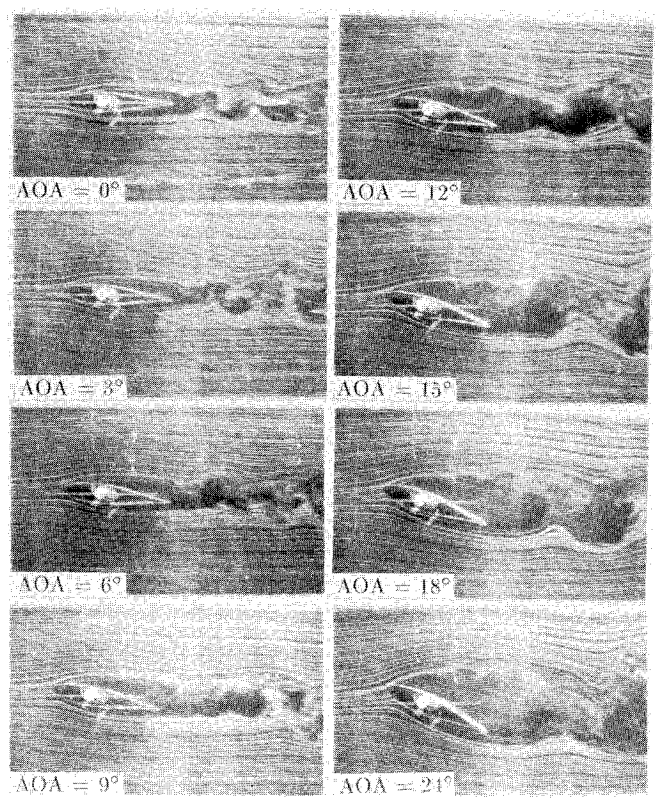

Fig. 4 Flow patterns for $Re_c = 15{,}400$.

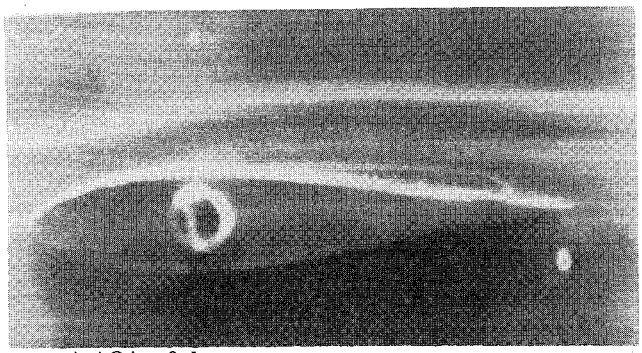

a) AOA = 0 deg

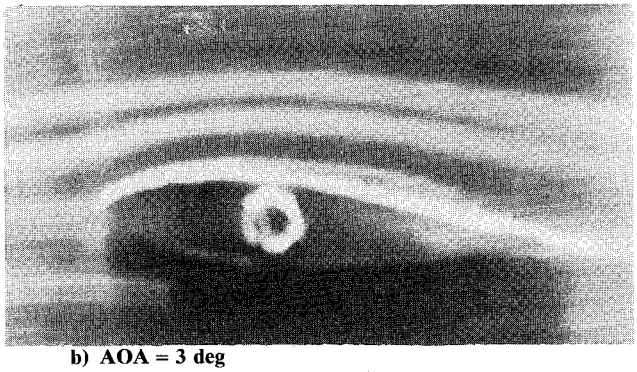

b) AOA = 3 deg

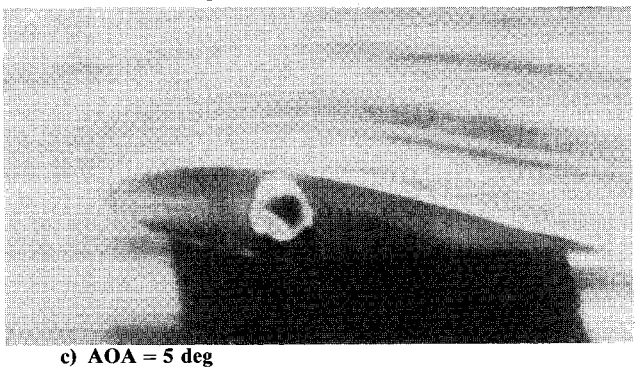

c) AOA = 5 deg

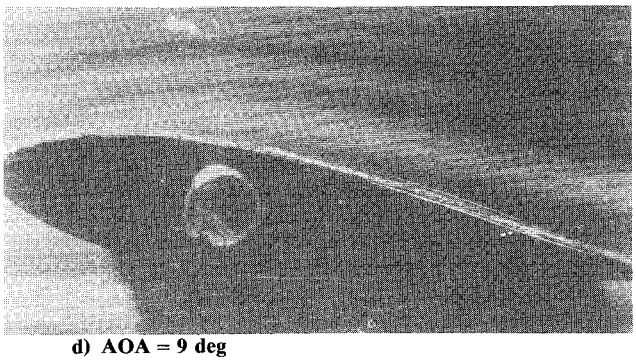

d) AOA = 9 deg

Fig. 5 Flow patterns for $Re_c = 55{,}000$.

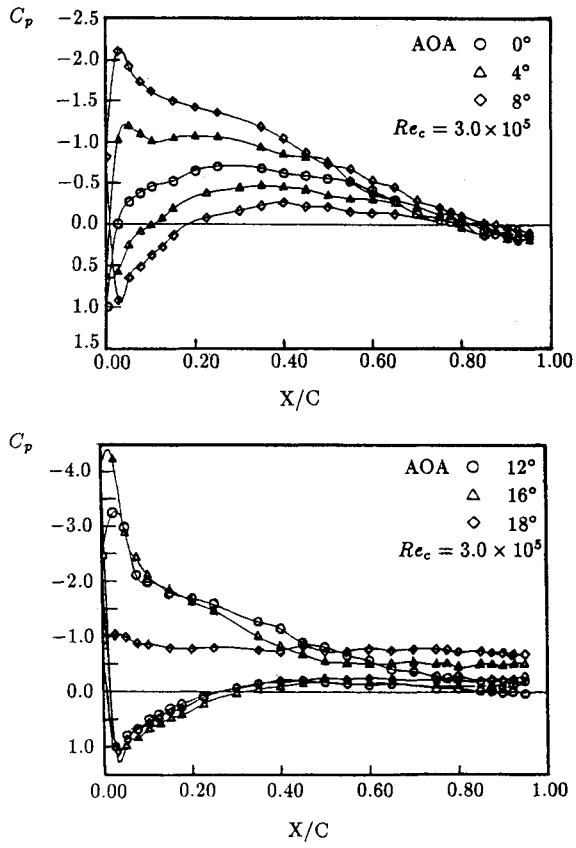

Fig. 6 Pressure distributions along the chord.

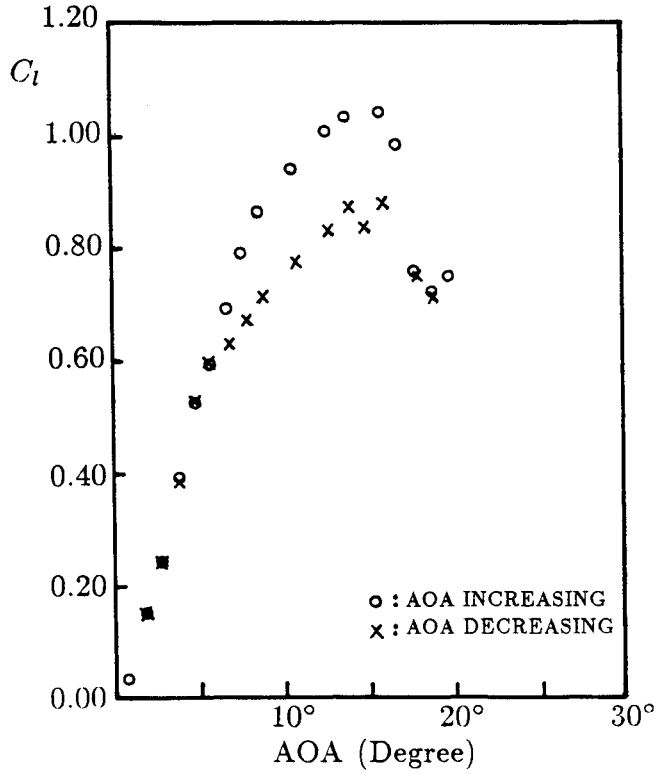

Fig. 7 Section lift coefficient curve with angle of attack for $Re_c = 300{,}000$.

number of 300,000. It is observed that after the minimum pressure point near the leading edge, the pressure gradient becomes positive, and then a plateau exists for a distance. The aforementioned laminar separation bubble is manifested by a constant pressure plateau[3,4] ranged approximately between 20 to 55% chord at the angle of attack less than 4 deg. The plateau is shifted toward the leading edge and reduced somewhat in its apparent length at higher angle. For 12 deg angle-of-attack case, a short plateau is initiated at about 8% chord with the length less than 3% chord. The adverse pressure gradient then goes on until close to the trailing edge of the airfoil. The pressure distribution curves along with the boundary-layer velocity profiles can be used to estimate the separation bubble profiles. The details will be discussed later. At 18 deg angle of attack, the pressure distribution on the upper surface becomes very

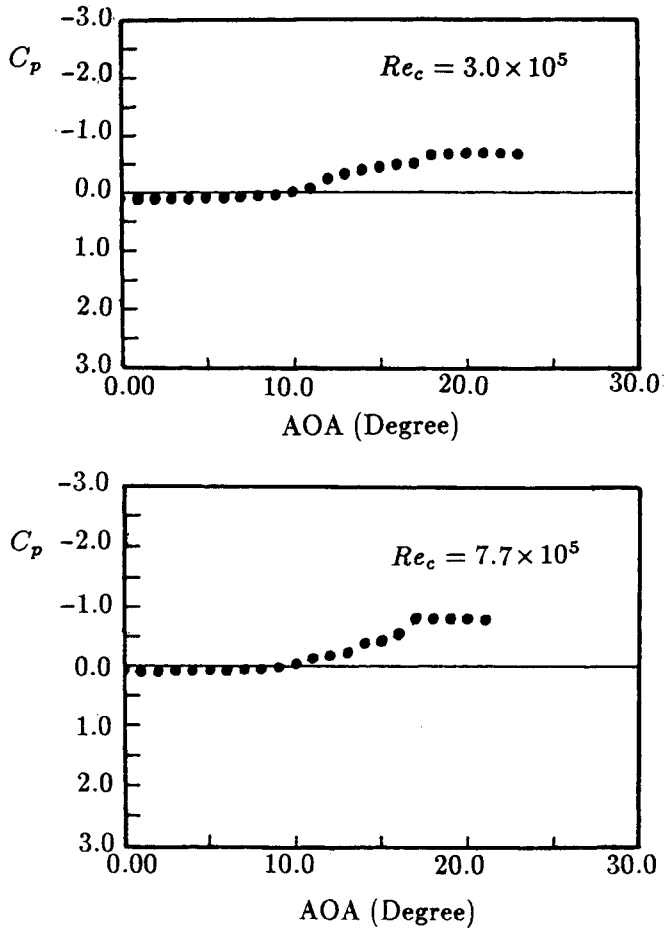

Fig. 8 Pressure coefficient with angle of attack at trailing edge.

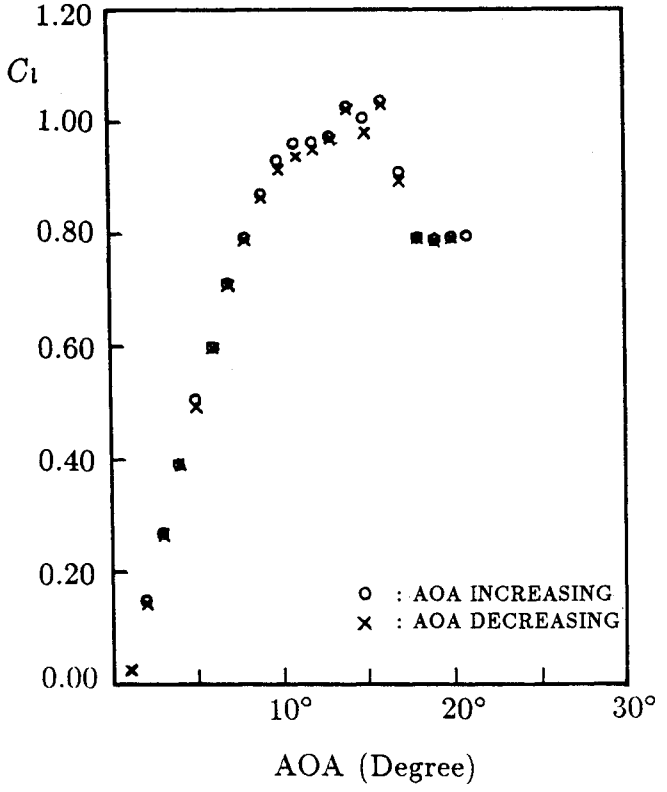

Fig. 9 Section lift coefficient curve with angle of attack for $Re_c = 774{,}000$.

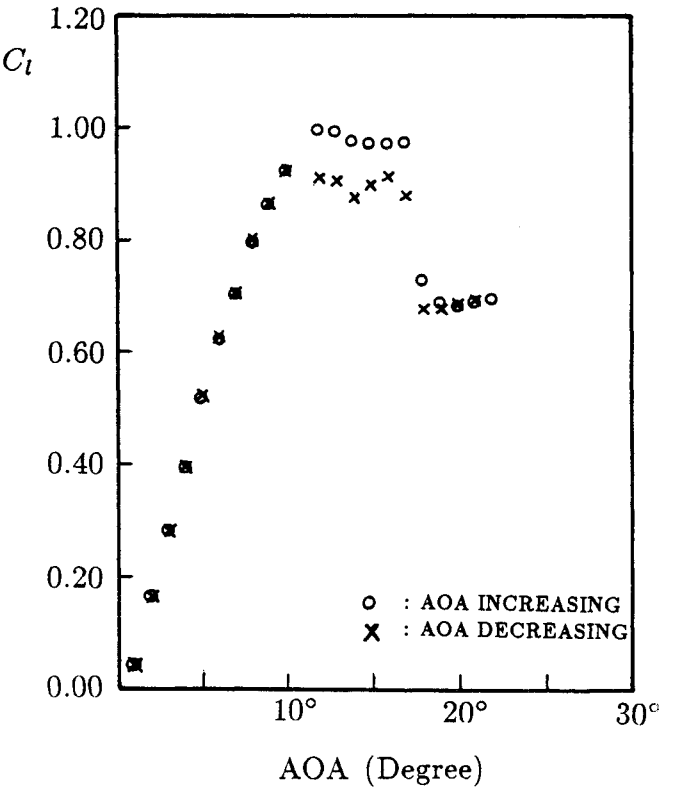

Fig. 10 Section lift coefficient curve with angle of attack for $Re_c = 659{,}000$.

flat, where the full stall has just occurred, as compared to the lift curve as shown in Fig. 7. For investigating the Kutta condition, a pressure tap is drilled right on the sharp trailing edge, which is supposed to be a stagnation point. Figure 8 shows the results of the pressure coefficients at the trailing edge with angle of attack for the Reynolds numbers of 300,000 and 774,000. They indicate that there exists a zero crossing at the angle of attack of 10 deg for both cases. The zero-crossing angle is about at the angle where the lift curve starts to be nonlinear. For even higher angle of attack, the pressure coefficient at the trailing edge becomes more negative and then saturates to a constant after full stall occurs beyond 18 deg angle of attack.

The section lift coefficient curves, obtained by integrating the pressure distributions, are plotted in Figs. 7, 9, and 10. The pressure information is acquired in the process when the change of the angle of attack is increased up to full stall. The process is then reversed until the zero deg angle of attack is reached. Regarding the wind-tunnel wall interference,[11] the actual lift coefficients are required to be corrected by reducing 3% from the measured data. The lift curves appear to be sensitive to the Reynolds number within the operating range. The value of the lift curve slope at the linear range is about 1.83π for all cases, which is close to the theoretical value of 2π for a two-dimensional thin airfoil. The phenomenon of the so-called hysteresis is not appreciable at the Reynolds number of 774,000, as shown in Fig. 9. But for the case of the Reynolds number being 659,000, as plotted in Fig. 10, a clockwise hysteresis loop is observed. Also, for the case when the Reynolds number reduces down to 300,000, as shown in Fig. 7, a more prominent hysteresis loop is presented as well. The occurrence of the hysteresis loop is explained as follows. For the process in increasing angle of attack from lower value, a laminar separation bubble is formed on the upper surface. It then moves upward and shrinks its size accordingly. Meanwhile, the turbulent separation point keeps moving toward the leading edge. The stall occurs when the turbulent separation point subsequently meets the bubble. At this moment, the bubble is destroyed and the reattachment no longer exists. That is, only the

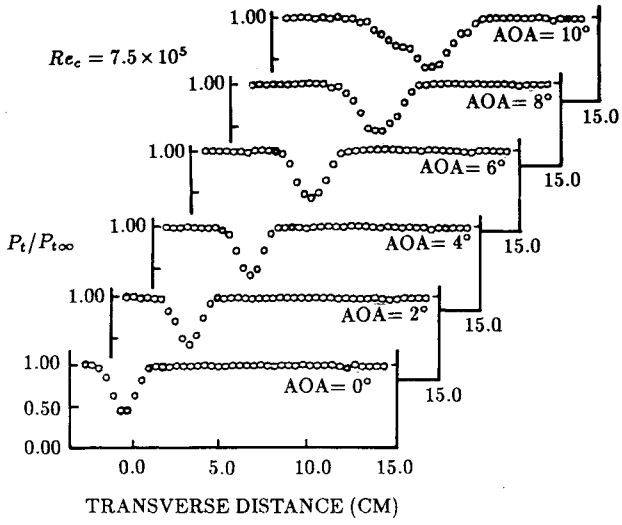

Fig. 11 Wake defect profiles for $Re_c = 750{,}000$.

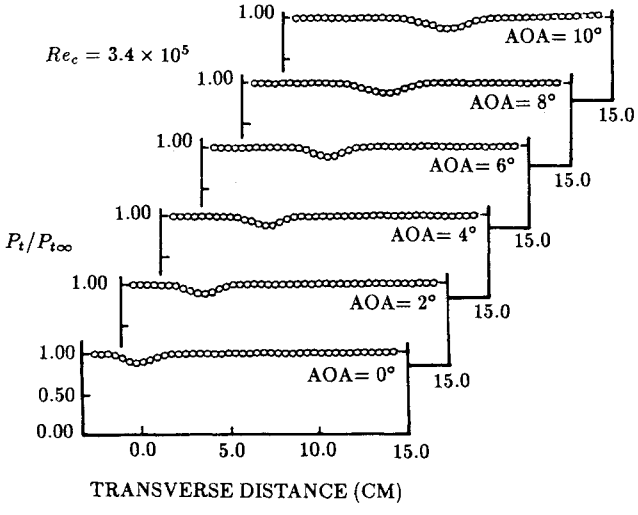

Fig. 12 Wake defect profiles for $Re_c = 340{,}000$.

leading-edge separation is presented. On the contrary, for decreasing angle of attack case from stall, the laminar separation bubble is not restored immediately. The bubble can only be reformed at somewhat lower angle of attack where the hysteresis loop is closed. Certain researchers[3,5,7] have also obtained the similar phenomenon in their different airfoils. In order to determine section drag coefficient, a wake survey method is employed. Figures 11 and 12 show a series of wake defect profiles for the angle of attack lower than 10 deg at Reynolds numbers of 750,000 and 340,000, respectively. For the cases of angle of attack higher than 10 deg, the wake survey method becomes doubtful because an abundant quantity of large-scale vortices are shedded into the wake region. The section drag coefficients for angles of attack less than 10 deg, measured by this technique, are shown in Fig. 13. The data reveal that the drag coefficient is quite insensitive within the operating Reynolds number range. Even compared with the case[12] for the Reynolds number of 5,800,000, the value does not change too much, except at the lower angles of attack.

Boundary-Layer Velocity Profiles and Separation Bubbles

The boundary-layer mean velocity profiles are obtained by traversing a flattened 0.2 mm opening total-pressure tube. Figures 14 and 15 illustrate the boundary-layer developments at angles of attack of 6 and 10 deg, respectively, for the Reynolds

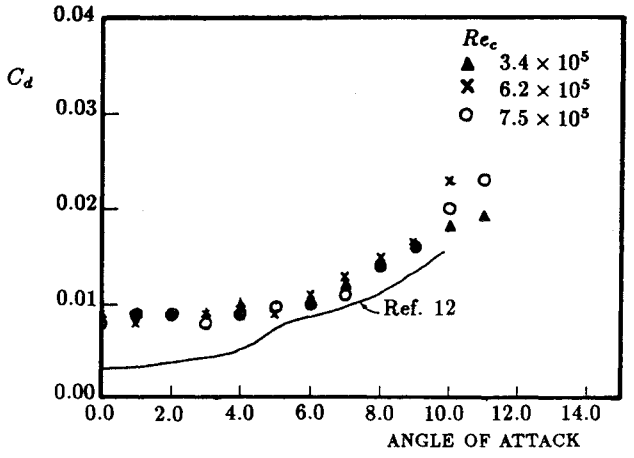

Fig. 13 Section drag coefficient curves with angle of attack.

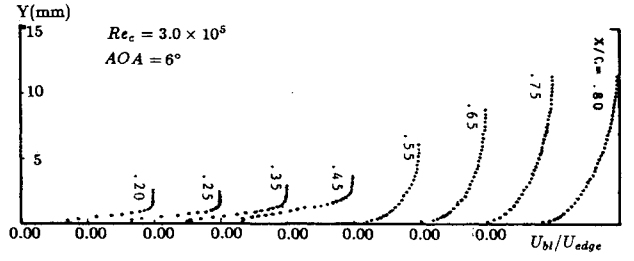

Fig. 14 Boundary-layer velocity profiles along the chord for angle of attack = 6 deg.

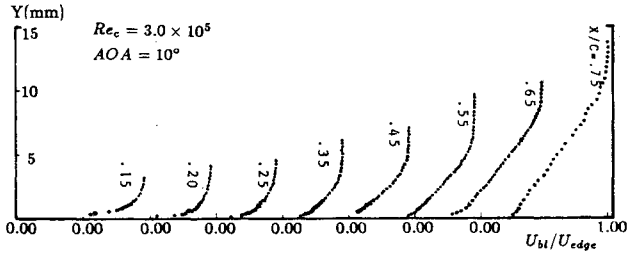

Fig. 15 Boundary-layer velocity profiles along the chord for angle of attack = 10 deg.

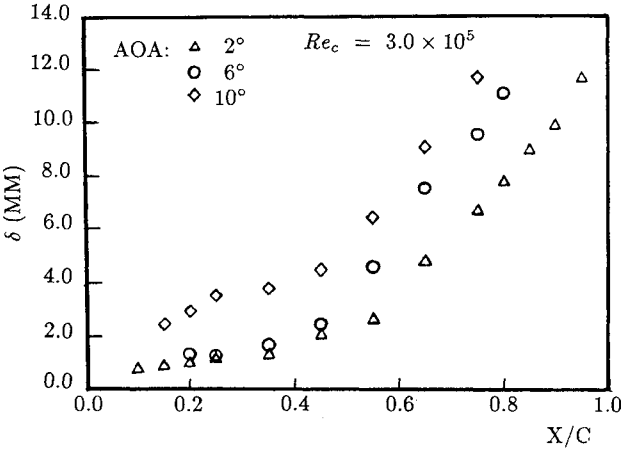

Fig. 16 Boundary-layer thickness along the chord.

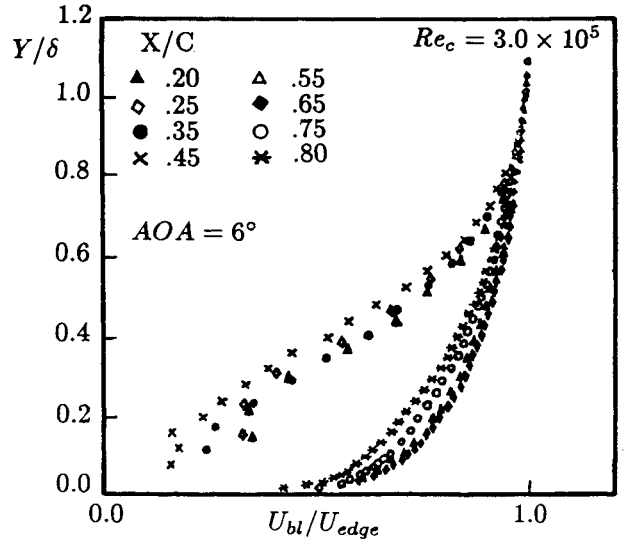

Fig. 17 Normalized boundary-layer velocity profiles for angle of attack = 6 deg.

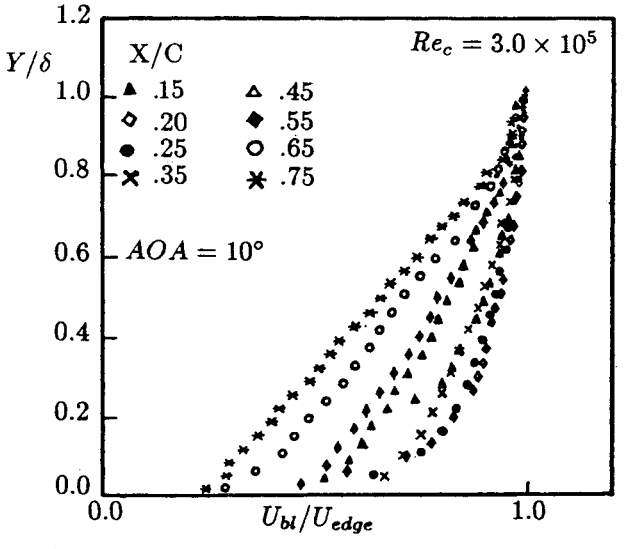

Fig. 18 Normalized boundary-layer velocity profiles for angle of attack = 10 deg.

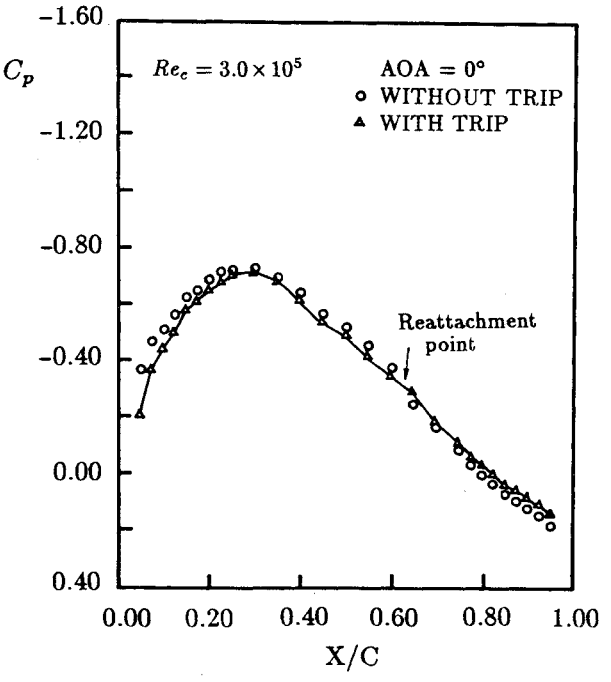

Fig. 19 Tripped and untripped pressure distributions along the chord for angle of attack = 0 deg.

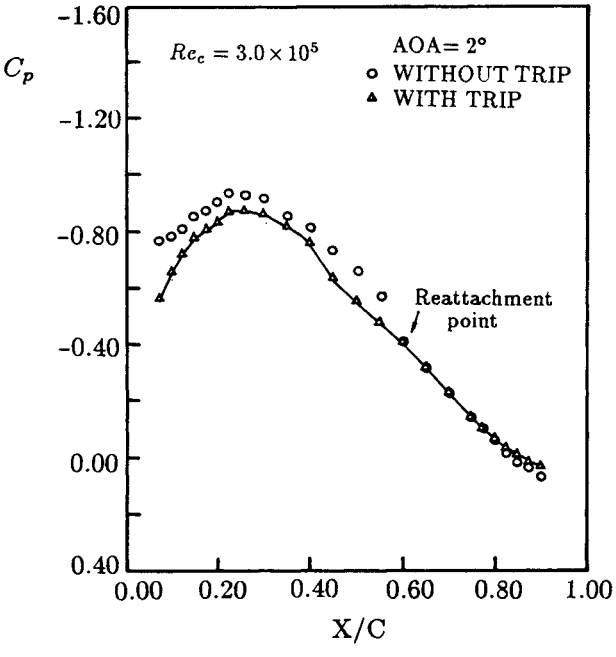

Fig. 20 Tripped and untripped pressure distributions along the chord for angle of attack = 2 deg.

number of 300,000. The boundary-layer thickness is defined as the distance from the wall to the point where the velocity reaches 99% of its edge velocity. The boundary-layer thickness with chordwise direction is shown in Fig. 16. It is clear that the boundary layer is getting thicker with the increase of angle of attack. By proper choice of the normalization factors, the normalized boundary-layer velocity profiles are replotted and shown in Figs. 17 and 18. For the 6 deg angle-of-attack case (Fig. 17), the data seem to be well collapsed into two relevant branches with 45 to 55% chord as the demarcation zone. That is, the velocity profiles taken before 45% chord are fitted into one branch, and those taken after 55% chord are fitted into the other branch. By checking the velocity gradient of these profiles, the two branches may be recognized as a laminar and a turbulent boundary layer, respectively.[11] The reattachment point is located right between these two branches. However, for 10 deg angle-of-attack case, the normalized velocity profiles look more scattered. From the pressure measurement as shown in Fig. 6, the reattachment point can be estimated to be at about 15% chord. Based on this, the data plotted in Fig. 18 are all in turbulent region. This is a reason why the data before 35% chord are fitted into a turbulent branch. But beyond 45% chord, the data start to be deviate. It is felt that the turbulent boundary-layer separation may play an important role in the flowfield now.

In order to identify the reattachment point, a tripping wire is employed to trigger the transition and suppress the laminar separation.[13,14] It is suggested[3] that the reattachment occurs when the pressure is nearly equal to the value for the turbulent boundary layer over the airfoil with no separation bubble present. By deploying a 1.5 mm diam wire spanning the whole model around the leading edge, the pressure distributions are measured to compare with those when untripped. Results are plotted in Figs. 19–22 for different angles of attack. The solid line represents the results when the flow is being tripped. For

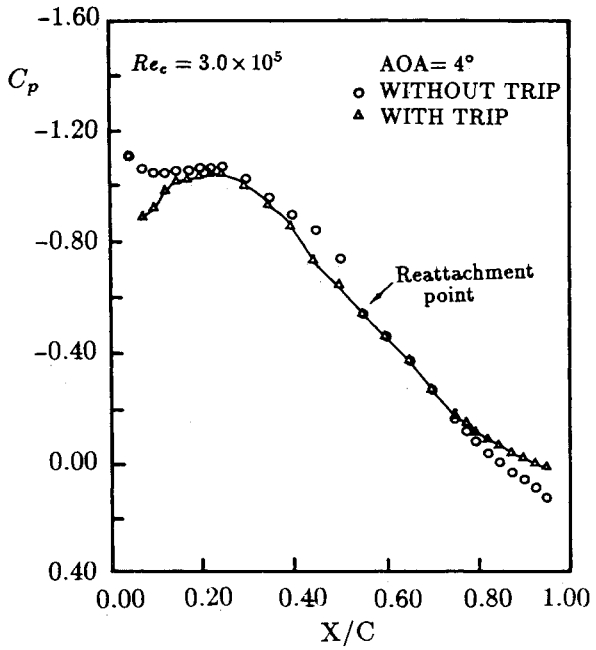

Fig. 21 Tripped and untripped pressure distributions along the chord for angle of attack = 4 deg.

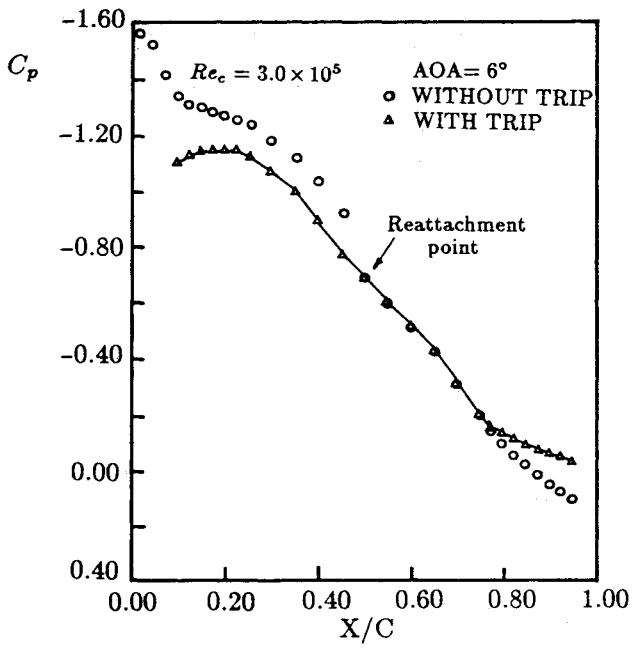

Fig. 22 Tripped and untripped pressure distributions along the chord for angle of attack = 6 deg.

the case of zero deg angle of attack in Fig. 19, two sets of data come across each other at 65% chord. It is then moved to 60% chord, 55% chord, and 50% chord for the angles of attack of 2, 4, and 6 deg, respectively. It is noted that the reattachment point is moving toward the leading edge with increasing angle of attack. By examining the normalized velocity profiles and pressure distribution curves, the location of reattachment points are quite consistent with each other.

Because of the flow being reversed inside the bubble, it is quite ambiguous to determine the separation bubble size if one directly examines the hot-wire velocity signal alone. LeBlanc et al.[4] suggested a method to estimate the separation bubble thickness, which stated that the height of the bubble was chosen to be the distance from the wall to the point where the boundary-layer velocity reaches 30% of its edge velocity. Unfortunately, it was not justified in their paper. We then examine the criterion by calculating the possible bubble heights at various percents of the edge velocity. The result is indicated in Fig. 23a. Without any further evidence, it is difficult to tell which one would be the appropriate bubble height. In order to resolve this ambiguity, the bubble is visualized by smoke wire technique along with boundary-layer velocity measurement. It is found that the velocity at the bubble boundary is about 75% of its edge velocity. This criterion is further reconfirmed by performing the spectral analysis. As one knows, the shear layer instability waves and the recirculating flow inside the bubble would contain some significant dominating frequencies. We then carry out velocity spectral evolution studies along the transverse direction at the maximum bubble height location, i.e., 45% chord. In inspecting these spectra as depicted in Fig. 25, there exists no clear frequency peaks, except that the distance is less than 1.5 mm in which the velocity corresponds to about 75% of the edge velocity. Having the evidence justified, the bubble boundary is taken to be at the location where the velocity equals 75% of the boundary-layer edge velocity. Figure 23b shows the result of the bubble profiles at various angles of attack according to the proposed criterion. As may be seen, the bubble is shifted toward the leading edge with increasing angle of attack. By observing the pressure coefficient distributions (Fig. 6) together with the corresponding velocity profiles (Fig. 14), the results of the bubble length estimation are quite consistent. For the current airfoil chosen, the bubble length seems to be elongated at lower angle of attack and then shrunk at higher angle of attack until the bubble is broken up.

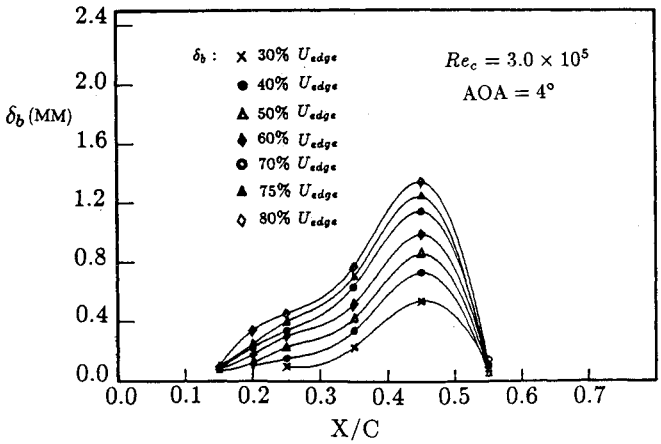

Fig. 23a Possible separation bubble profiles for different percents of edge velocity.

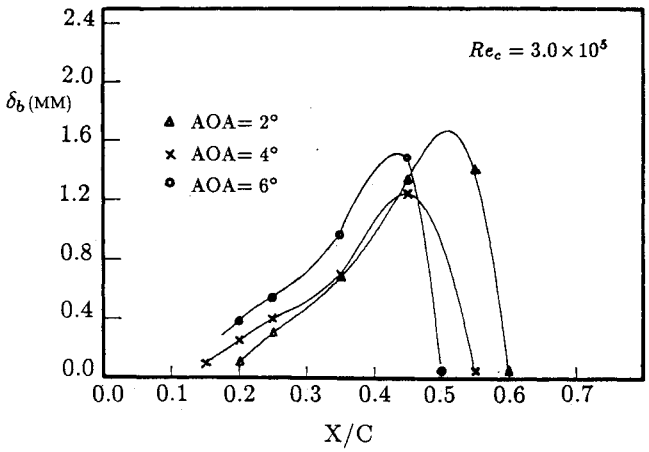

Fig. 23b Measured separation bubble profiles for certain angle of attack.

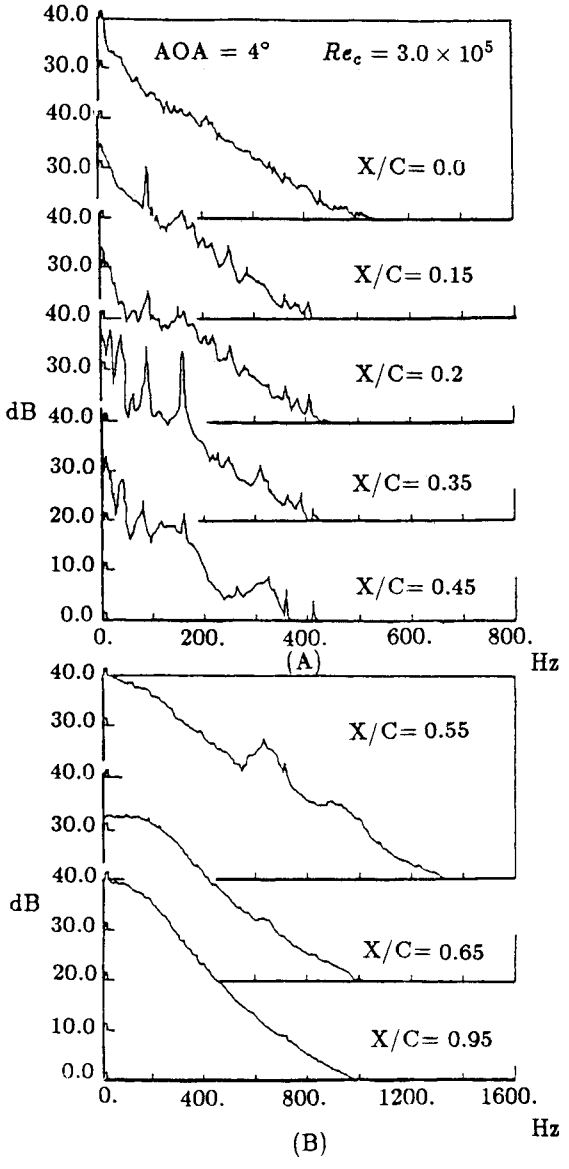

Fig. 24 Boundary-layer velocity spectra for specific chordwise location dB = 20 log(V/1.0 V).

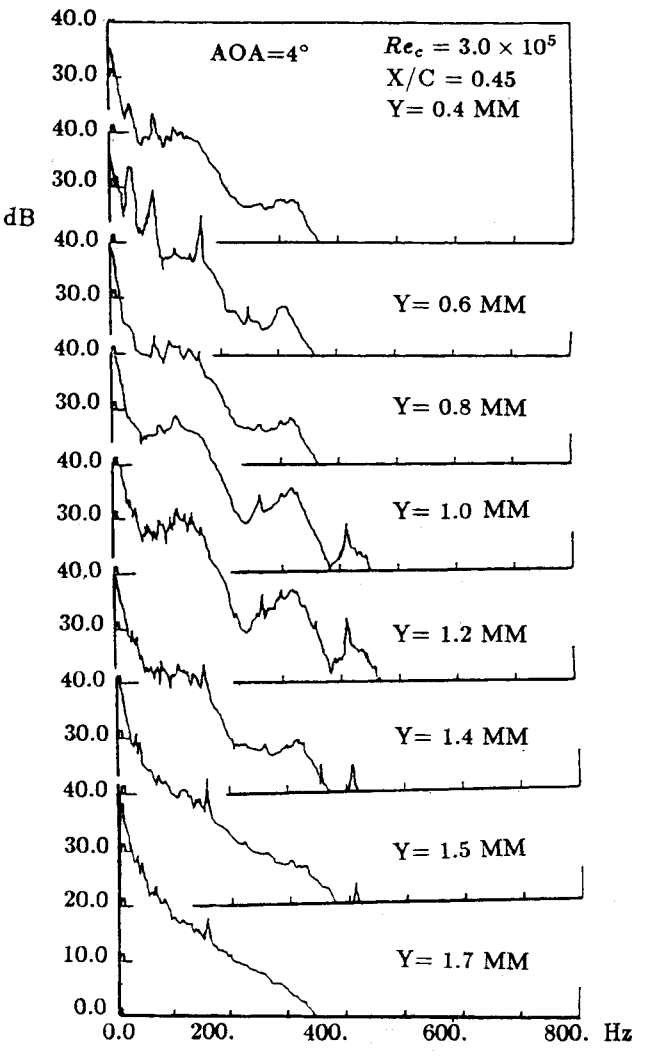

Fig. 25 Boundary-layer velocity spectra for specific transverse location at 45% chord dB = 20 log(V/1.0 V).

Fluctuating Energy Spectra Evolution

To investigate the flow structures during the presence of the bubble on the upper surface, the energy spectral analysis of streamwise velocity fluctuations via Fast Fourier Transform is carried out to determine the dominant peaks and their energy-contained developments of eddies.[15,16] A single hot wire is traversed along the upper boundary-layer surface of the model to map out the whole flowfield. The fluctuating velocity signals in voltage are fed directly into the spectrum analyzer. Some of the interesting results are shown in Figs. 24 and 25 for 4 deg angle of attack and 300,000 Reynolds number. It is noted that the ordinate is expressed in decibels with a reference voltage of 1 V. Since the main purpose of the spectral analysis is to identify the dominant frequency peaks of the flow structures, the reference voltage can be chosen at one's convenience. That is, the prevailing eddies will be presented by the pronounced frequency peaks. Figures 24a and 24b have the same feature except for the difference in frequency domain. They depict the energy spectra evolution of the eddy structures along the chordwise direction at maximum velocity fluctuations. There exists no clear peak in the freestream spectrum. But when moving to 15% chord location, a prominent peak of 97 Hz is sprouted and keeps surviving until reaching the 45% chord. Two more clear peaks of 32 and 153 Hz are also manifested at 35% chord and at 45% chord as well. However, at 55% chord, all of the above peaks vanish and an even higher peak, 634 Hz, appears. But when moving further toward the trailing edge, the peak then fades away. As discussed before, we have determined that for the same condition the reattachment point is located around 55% chord. Comparison with the present spectra results suggests that the existence of the dominant peaks evidently is related to the presence of the separation bubble. In particular, these low-frequency eddies that prevailed from 15 to 35% chord are associated with the relatively slow-moving portion of the separation bubble which occupies before the transition, as noted by O'Meara and Mueller.[17] Also, the high-frequency eddies after 45% chord are subjected to the rear portion of the bubble where the flow approaches the reattachment and will be more turbulent. Figure 25 presents the spectral development in the transverse direction at 45% chord where the bubble height is maximum (Fig. 23a). The same feature of low-frequency peaks are observed inside the bubble under the height of 0.6 mm. Another prevailing high-frequency peak, 320 Hz, takes place right beyond that height. It seems that the peak frequency is somehow related to the peak of 630 Hz, as discussed in Fig. 24. Meanwhile, there exists no prominent peak in the spectrum above 1.5 mm. In association with the boundary-layer profiles measurement as mentioned earlier, this substantiates the criterion for describing the bubble profile.

Concluding Remarks

For the NACA 63_3-018 airfoil investigated, the separation bubble is significant when present by flow visualization at the Reynolds number of 55,000, which is beyond the subcritical range. The bubble profile is further studied by performing the measurements of pressure distributions, boundary-layer velocity profiles, spectral analysis of fluctuating velocity, and reattachment point identification via the application of tripping technique in the Reynolds number range from 300,000 to 774,000. Results deduced from these different sources are quite consistent for describing the bubble properties. A criterion for determining the bubble height is proposed to be at the location where the boundary layer reaches 75% of its edge velocity. Moreover, the length of the bubble is subjected to the Reynolds number and the angle of attack. For the model tested, the bubble length increases with angle of attack up to 6 deg and then decreases with increasing angle of attack until the bubble vanishes.

The velocity spectra surveying around the bubble not only approves the criterion for describing the bubble profile but also suggests the existence of the prevailing eddies, especially inside the bubble. However, the front portion of the bubble moves slower since it contains relatively lower frequency peaks compared with the rear portion of the bubble.

The hysteresis phenomenon in the section lift curves with angle of attack is clearly observed and sensitive to the Reynolds number. Its loop size becomes smaller with the increase of the Reynolds number, whereas the loop has disappeared at the Reynolds number of 774,000. The drag coefficient obtained from the wake rake measurement seems to be insensitive in the operating Reynolds number range.

Acknowledgment

This work is supported by the National Science Council, Republic of China, under the Contract NSC 75-0401-E006-13.

References

[1]Maughmer, M. D. and Selig, M. S., "Low Reynolds Number Airfoil Design," *Proceedings of the Conference on Low Reynolds Number Airfoil Aerodynamics,* Univ. of Notre Dame, South Bend, IN, UNDAS-CP-77B123, June 1985, pp. 15–26.

[2]Lissaman, P. B. S., "Low Reynolds Number Airfoils," *Annual Review of Fluid Mechanics*, Vol. 15, 1983, pp. 223–239.

[3]Mueller, T. J., "Low Reynolds Number Vehicles," edited by E. Reshotko, AGARD-AG-288, Feb. 1985.

[4]LeBlanc, P., Liebeck, R. H., and Blackwelder, R., "Boundary Layer and Performance Characteristics from Wind Tunnel Tests of a Low Reynolds Number Liebeck Airfoil," *Proceedings of the Aerodynamics at Low Reynolds Numbers*, The Royal Aeronautical Society, London, Vol. 1, Oct. 1986, pp. 8.1–8.19.

[5]Mueller, T. J., "The Influence of Laminar Separation and Transition on Low Reynolds Number Airfoil Hysteresis," *Journal of Aircraft*, Vol. 22, Sept. 1985, pp. 763–770.

[6]Schmidt, G. S., O'Meara, M. M., and Mueller, T. J., "An Analysis of a Separation Bubble Transition Criterion at Low Reynolds Numbers," *Proceedings of the Conference on the Low Reynolds Number Airfoil Aerodynamics,* Univ. of Notre Dame, South Bend, IN, UNDAS-CP-77B123, June 1985, pp. 125–136.

[7]Marchman, J. F., "Aerodynamic Testing at Low Reynolds Number," *Journal of Aircraft*, Vol. 24, Feb. 1987, pp. 107–114.

[8]Harvey, W. D., "Low Reynolds Number Aerodynamic Research at NASA Langley Research Center," *Proceedings of the Conference on Aerodynamics at Low Reynolds Numbers*, The Royal Aeronautical Society, London, Vol. 2, Oct. 1986, pp. 19.1–19.49.

[9]Eppler, R., "Recent Developments in Boundary Layer Computation," *Proceedings of the Conference on Aerodynamics at Low Reynolds Numbers*, The Royal Aeronautical Society, London, Vol. 2, Oct. 1986, pp. 12.1–12.18.

[10]Cebeci, T., Wang, G. S., Chang, K. C., and Choi, J., "Recent Developments in the Calculation of Flow Over Low Reynolds Number Airfoils," *Proceedings of the Conference on Aerodynamics at Low Reynolds Numbers*, The Royal Aeronautical Society, London, Vol. 2, Oct. 1986, pp. 15.1–15.13.

[11]Pope, A. and Harper, J. J., *Low Speed Wind Tunnel Testing*, 2nd. ed., Wiley, New York, 1984.

[12]McCullough, G. B. and Gault, D. E., "Examples of Three Representative Types of Airfoil-Section Stall at Low Speed," NACA TN-2502, 1951.

[13]Mangalam, S. M., Bar-Sever, A., Zaman, K. B. M. Q., and Harvey, W. D., "Transition and Separation Control on a Low Reynolds Number Airfoil," *Proceedings of the Conference on Aerodynamics at Low Reynolds Numbers*, The Royal Aeronautical Society, London, Vol. 1, Oct. 1986, pp. 10.1–10.19.

[14]Gleyzes, C., Cousteix, J., and Bonnet, J. L., "Theoretical and Experimental Study of Low Reynolds Number Transitional Separation Bubbles," *Proceedings of the Conference on Low Reynolds Number Airfoil Aerodynamics,* Univ. of Notre Dame, South Bend, IN, UNDAS-CP-77B123, June 1985, pp. 137–152.

[15]Fisher, S. S. and Horger, D. C., "Smoke-Wire and Thin-Film-Gauge Observations of Laminar Separation Bubbles on NACA 23012-64 Airfoil Section," *Proceedings of the Conference on Aerodynamics at Low Reynolds Numbers*, The Royal Aeronautical Society, London, Vol. 3, Oct. 1986, pp. 36.1–36.24.

[16]Corke, T. C. and Morkovin, M. V., "On Effect of Three Dimensional Roughness on Transition and Receptivity to Disturbances," *Proceedings of the Conference on Low Reynolds Number Airfoil Aerodynamics,* Univ. of Notre Dame, South Bend, IN, UNDAS-CP-77B123, June 1985, pp. 293–306.

[17]O'Meara, M. M. and Mueller, T. J., "Laminar Separation Bubble Characteristics on an Airfoil at Low Reynolds Numbers," *AIAA Journal*, Vol. 25, Aug. 1987, pp. 1033–1041.